



# Exploring the interplay between observed warming, atmospheric circulation, and soil-atmosphere feedbacks on heatwaves in a temperate mountain region

Marc Lemus-Canovas<sup>1,2</sup>, Sergi Gonzalez-Herrero<sup>3</sup>, Laura Traperó<sup>2</sup>, Anna Albalat<sup>2</sup>, Damian Insua-Costa<sup>4,1</sup>, Martin Senande-Rivera<sup>5</sup>, Gonzalo Miguez-Macho<sup>5</sup>

<sup>1</sup>Center for Climate Change and Transformation, Eurac Research, Bozen/Bolzano, 39100, Italy. <sup>2</sup>Andorra Research + Innovation, Sant Julià De Lòria, AD600, Andorra. <sup>3</sup>WSL Institute for Snow and Avalanche Research (SLF) Davos, CH-7260, Switzerland. <sup>4</sup>Hydro-Climate Extremes Lab (H-CEL), Ghent University, Ghent, Belgium. <sup>5</sup>CRETUS, Non-linear Physics Group, Universidade de Santiago de Compostela, 15782, Spain.

*Correspondence to:* Marc Lemus-Canovas (marc.lemusicanovas@eurac.edu)

**Abstract.** This study investigates the exceptional heatwaves of 2022 in the Pyrenees, focusing on their physical drivers and environmental influences. The June heatwave was advective in nature, with stronger mountain-induced circulations resulting in heterogeneous temperature anomalies, while the July event had subsiding and weaker atmospheric flow, leading to more uniform temperatures. The interplay of the synoptic circulation with the complex topography, or the pre-existing soil moisture deficits, played an important role in driving the spatial variability of temperature anomalies in the heatwaves and contributed significantly to their regional amplification. In addition, human-induced climate change has exacerbated these extreme weather phenomena, with more intense heatwaves in the recent period (1986-2021) compared with the past (1950-1985). This research contributes to a more realistic assessment of the impact of climate change on heatwaves in mountain regions.

## 1 Introduction

The Pyrenees constitute one of the southernmost alpine mountain ranges in Europe and they are prone to severe heatwaves due to their location in a climatic transition zone between the humid temperate domain of higher latitudes and the dry warm domain of subtropical latitudes. Numerous observation-based studies in this region have shown a consistent temperature increase during the last few decades, across all seasons (Perez-Zanón, 2017; Moreno et al., 2018; Lemus-Canovas & Lopez-Bustins, 2021). The observed changes in temperature increase have already impacted ecosystems (Camarero, 2017; Gazol et al., 2020) leading to a reduction in snow cover and ice mass loss (Lopez-Moreno et al., 2016; Lopez-Moreno et al. 2020; Vidaller et al., 2021), among other effects.

Despite the observed upward trend in mean temperatures, the relationship between specific extreme temperature events -such as the 2022 summer heatwaves- and global warming has not yet been thoroughly investigated in the Pyrenees. Studies from other regions (Barriopedro et al., 2020, Yiou et al., 2020, Xu et al., 2021; White et al., 2023) have demonstrated that



extreme temperatures are often associated with significant anomalies in large-scale atmospheric circulation patterns. In southwestern Europe, where the Pyrenees are located, high temperature episodes or heat waves are usually driven by subtropical high-pressure systems known as subtropical ridges (Garcia-Herrera et al., 2005). These systems manifest as narrow bands of positive geopotential height anomalies extending from subtropical latitudes into southern Europe (Sousa et al. 2018). Prolonged periods of elevated geopotential heights promote atmospheric subsidence, leading to substantial adiabatic warming and increased surface radiative fluxes (Zschenderlein et al., 2019). Such adiabatic processes allow for the maintenance of high surface temperatures during heatwaves, as observed in numerous studies in different regions (Miralles et al., 2014; Sousa et al., 2019; Zschenderlein et al., 2019; Gonzalez-Herrero et al. 2022, among others). Heatwaves can be also intensified by land-atmospheric coupling effects. Soil with low moisture prior to a heatwave event can exacerbate extreme conditions as latent heat fluxes are reduced and sensible heat fluxes increase, which in turn reduces evaporative cooling and thus increases air temperature (Fischer et al., 2007; Seneviratne et al., 2010). The contribution of very dry soil to the intensification of heatwaves has been demonstrated at both large scales and in specific events (Miralles et al., 2014; Schumacher et al., 2019; Sousa et al., 2020), such as the 2010 and 2018 heatwaves in Europe. However, a more local approach is lacking for mountain areas and their surrounding regions.

In this study we focus on two heat waves that occurred in the summer of 2022, one in June and one in July, which broke several temperature records in Western Europe (Witze, 2022; Yule et al., 2023; Serrano-Notivoli et al., 2023) and had severe impacts on ecosystems, such as provoking an acute wildfire outbreak in Spain (Rodrigues et al., 2023), or causing extreme glacial melting in Switzerland (Cremona et al., 2023). The Pyrenees area was no exception in the context of summer 2022. Both the duration and, especially, the intensity of heatwaves associated with this extremely warm season were unprecedented in this mountain system and its surrounding areas (Figure 1a). Therefore, the specific objectives of the present study are: (1) to assess the physical mechanisms that contributed to the two extreme heatwaves of summer 2022 in the Pyrenees and surrounding areas, (2) to examine the role of climate change in these heatwaves that made this summer the warmest on record (1950-2022) and (3) based on reanalysis data and observations, to study the soil-atmosphere feedbacks during these events and analyze the possible differential temperature amplification induced by them in the study region.

## 2 Data and methods

### 2.1 Data

Daily minimum and maximum 2 m temperature (hereafter,  $T_x$  and  $T_n$ , respectively) were extracted from the European Centre of Medium-range Weather Forecast (ECMWF) ERA-5 Land reanalysis (Copernicus Climate Change Service, C3S, Muñoz-Sabater et al., 2021). These variables were used to characterize anomalies and extremes during the 2022 events, as well as to compute the heatwave (HW) algorithm. In addition,  $T_x$  was used as a predictand in the analogue's exercises. Apart from temperature data, volumetric soil moisture (in  $\text{m}^3 \text{m}^{-3}$ ) in a layer of 0 to 7 cm depth (swl1) was also retrieved and used for computing anomalies and for the analogue exercise, with respect to the climatological seasonal cycle (1950–2021).



65 Finally, cumulative daily surface solar and thermal net radiation ( $R_n$ ), evaporation ( $E$ ) and potential evaporation ( $E_p$ ) were  
employed to examine land-atmosphere interactions during HW events. Meteorological fields for atmospheric levels were  
retrieved from the ERA-5 reanalysis daily dataset (Hersbach et al., 2020), starting in 1950. The following variables were  
considered on a  $0.25^\circ \times 0.25^\circ$  horizontal resolution grid for the pressure levels comprised between 1000 and 500 hPa: air  
temperature, potential temperature, geopotential height, zonal/meridional wind components, vertical velocity. These fields  
were used to: (i) characterize the synoptic drivers of both HWs, (ii) generate vertical profiles, (iii) compute the contributing  
70 terms to the temperature tendency equation, and (iv) perform the analogue exercises. Specific methods for products derived  
from these variables are explained below. In all cases, anomalies were also computed with respect to the climatological  
seasonal cycle (1950–2021).

For validation purposes,  $T_x$  of the summer season (JJA) was extracted from the database of the CLIMPY project  
(Characterization of the evolution of climate and provision of information for adaptation in the Pyrenees); this cross-border  
75 initiative aimed to perform a comprehensive analysis of recent trends in temperature, precipitation and snow cover in the  
Pyrenees, as well as their future projection (Cuadrat et al., 2020). Data for these variables were provided on a high-resolution  
grid of  $1 \text{ km} \times 1 \text{ km}$ , covering the period 1981–2015. This dataset was derived from observations collected at 1343 weather  
stations located in Andorra, France and Spain; the grid was developed following the quality control, reconstruction and  
gridding processes outlined by Serrano-Notivol et al. (2017; 2019). Finally, three in situ weather stations time series of daily  
80  $T_x$  and total precipitation located in Huesca (Aragon, Spain), Encamp (Andorra) and Tarbes (Hautes-Pyrénées, France) were  
retrieved from Spanish National Meteorology Agency (AEMET), FEDA (Forces Elèctriques d'Andorra), and the European  
Climate Assessment & Dataset (ECA&D), respectively. Three stations comprise the period 1950–2022. As mentioned above,  
both CLIMPY grid and in-situ stations were used to support the results obtained through ERA5-Land.

## 2.2 Methods

### 85 2.2.1 Heatwave definition

Heatwaves were defined as periods of three or more consecutive days with daily  $T_x$  and  $T_n$  values above the climatological  
(1950–2021) 99th percentile, calculated based on a 31-day moving window centered in the specific calendar day, following a  
similar approach as Russo et al., (2014). The heatwave incidence per summer season (June–August 1950–2022) was  
explored by accounting both heatwave duration and heat intensity. The intensity indicator was defined as the cumulative  
90 temperature anomaly during an event with respect to the abovementioned  $T_x$  and  $T_n$  climatological thresholds. This  
indicator was also provided annually by summing all the HW intensities recorded each summer season. For the attribution  
analysis, the two heatwaves of summer 2022 accumulating the greatest heat intensity were selected as study cases. To obtain  
the most geographically extensive heat waves, another criterion was used whereby at least 80% of the study area was  
affected by a heat wave situation.



## 95 2.2.2 Thermodynamic equation

We assessed the contribution of physical processes to preconditioning, build-up, maintenance and decay of the heatwaves using the thermodynamic equation:

$$\frac{\Delta T}{\Delta t} = \underbrace{-\vec{v} \cdot \nabla_p T}_{Adv} - \underbrace{\omega \frac{T}{\theta} \frac{\partial \theta}{\partial p}}_{Adiab} + \underbrace{Q}_{Diab} \quad (1)$$

where  $\vec{v}$  is the horizontal wind,  $T$  the temperature,  $\omega$  the vertical velocity in pressure coordinates,  $\theta$  the potential temperature and  $p$  the pressure. We evaluated equation 1 at 700 hPa in order to measure the processes that regionally affect the study area while avoiding surface effects and intersecting mountains. The left-hand side term represents the temperature tendency, while the right-hand side terms represent the horizontal advection, the adiabatic term and the diabatic processes, respectively. The first three terms were computed for every grid point in the Pyrenees area and then averaged regionally. To compute the adiabatic vertical gradients, we used the fields at 750 and 850 hPa. The diabatic term was calculated as the residual of the other components and therefore might include other factors such numerical errors, and in general played a secondary role during the assessment of 2022 heatwaves.

## 2.2.3 Thermodynamic equation

To assess and quantify the magnitude of soil moisture–temperature coupling, we used the  $\pi$  diagnostic proposed by Miralles et al. (2012). This indicator estimates two terms based on near surface air temperature ( $T$ ), evaporation ( $E$ ), potential evaporation ( $Ep$ ) and surface net radiation ( $Rn$ ). The  $\pi$  metric is defined as the product of a standardised temperature term ( $T'$ ) and energy term ( $H' - Hp'$ ).

$$\pi = (H' - Hp') T', \quad (2)$$

where  $H'$  represents the actual sensible heat derived from the estimated evaporation and surface net radiation, and  $Hp'$  denotes the sensible heat that would occur under potential evaporation. Both  $H'$  and  $Hp'$  are expressed as standard deviations relative to their expected mean.

$$(H' - Hp') = (Rn - \lambda E)' - (Rn - \lambda Ep)'. \quad (3)$$

Here,  $\lambda E$  is the latent heat flux of vaporization, calculated as a function of  $T$  and  $Rn$  following *Priestley and Taylor (1972)*. The energy term ( $H' - Hp'$ ) effectively represents the short-term potential of soil moisture to influence  $T$  by altering the partitioning of available radiative energy. When soil moisture is sufficient to meet the atmospheric demand for water, evaporation equals the potential evaporation, and the energy term is zero. Under dry conditions, as atmospheric water demand increases and soil moisture gradually decreases, the energy term increases. Consequently, the soil moisture–temperature coupling ( $\pi$ ) attains high values when positive values of  $T'$  co-occur with elevated levels of ( $H' - Hp'$ ). The  $\pi$  diagnostic was computed daily for each grid point during the summer season (JJA). The resulting spatial  $\pi$  time series was used in one of the analogue exercises and to draw a cross section to estimate the extent of the coupling across the study area for the 1950-2022 summer period.



#### 2.2.4 Flow analogues

We use the analogue approach, which infers the probability distribution of a target field from the atmospheric circulation during a considered time interval (Jézéquel et al., 2018). Here, two analogue experiments were designed for each heatwave event but with different target fields, one to examine climate warming attribution and the other to establish the role of soil moisture. They are explained in detail below. In both cases, flow analogue days are defined from their root-mean-square differences (RMSD) with respect to the actual z500 anomaly field at the time of the HW event over the following synoptic domain (30°–50°N, 20° W–10°E), centered on the Pyrenean domain (41.9°–43°N, 1.5°W–2.9°E, rectangle box in Fig.1e-1j). For each day of the considered HW event, the search of flow analogues was restricted to the boreal summer months (JJA), excluding the year of occurrence of the HW. Analogue days are used to reconstruct the target field by randomly picking one of the  $N$  best flow analogues for each day of the HW event. This reconstruction was repeated up to 5000 times. This  $N$  value was set to 30, being the ~1% of the sample size close to the event. For both analogue experiments, we employed z500 at the daily scale as a predictor in the flow analogues search. In all cases, anomalies were defined with respect to the 1950–2021 period.

In the first analogue experiment, we spatially reconstructed the expected mean  $T_x$  and  $\pi$  for each event and for both study periods: 1950–1985 and 1986–2021. In addition, we reconstructed the sw11 fraction for the 15-day period ([-15,-1] day interval) preceding each day of the June and July HW by using the same technique. Specifically, the flow-conditioned reconstructions of  $T_x$  and sw11 were also averaged over the Pyrenean domain for each subperiod. Since the atmospheric circulation is constrained, the differences between the past and present reconstructions can primarily be attributed to overall climatological variations between the two subperiods. To estimate the contribution of regional warming to the amplification of such events, we then repeated this flow analogue experiment by linearly removing the trend in z500 and  $T_x$ .

A second flow analogue experiment was based on the approach proposed by Sousa et al. (2020) to address whether the previously accumulated soil moisture deficits over the Pyrenean domain could have contributed to intensifying the temperature anomalies over that region at the time of the July HW. In this case, we reconstructed  $T_x$  anomalies expected from the circulation during the June and July HW, distinguishing between analogue days preceded by dry and wet conditions. Wet and dry conditions were defined as summer days of the full period with 15-day mean regional anomalies for the previous 15-day interval staying above the 66<sup>th</sup> percentile and below the 33<sup>rd</sup> percentile of the climatological sw11 distribution, respectively. In this way, soil moisture departures of a given analogue day represent previously accumulated values and are not the direct response to the actual atmospheric circulation conditions. To avoid the effects of long-term trends that may further complicate the causality of the relationships between soil moisture and temperature, these fields as well as z500 were detrended by linearly removing their trends. This second experiment was repeated by using the high-resolution  $T_x$  CLIMPY dataset, to provide a validation of the results obtained with ERA-5 Land. The results achieved with the later experiment were extended beyond the aforementioned Pyrenean domain in order to better understand the spatial patterns obtained.



### 3 Results

#### 160 3.1 The two extreme warm events and their associated atmospheric circulation

During the summer of 2022, successive heatwaves affected the Pyrenees reaching intensities never recorded in the instrumental data period in a 52% of its area (Fig. 1a). Additionally, 10% of the region experienced a record number of cumulative days in heat wave conditions. The most intense heatwaves occurred between June 12 to 19 (June Heatwave, June HW, Fig. S1a) and between July 15 to 19 (July Heatwave, July HW, Fig. S1b). These extreme heat events resulted in

165 positive near-surface maximum temperature ( $T_x$ ) anomalies ranging between  $6^{\circ}\text{C}$  and  $12^{\circ}\text{C}$  for the June event (Fig. 1e) and between  $9^{\circ}\text{C}$  and  $14^{\circ}\text{C}$  for the July event (Fig. 1f). These anomalies generated absolute record values in the Aquitaine Basin (Tarbes) (Fig. 1d) and mountainous areas such as Encamp in Andorra (Fig. 1b). The July HW (Fig. 1f) was the most intense of the summer, with  $T_x$  anomalies generally higher than those of the June HW (Fig. 1g). However, to the south and north of the mountain range, both HWs showed similar anomalies.

170 South of the Pyrenees, in the Ebro Valley, some precipitation was recorded during the period between the two heatwaves, yielding a higher volumetric soil moisture fraction between 0-7cm depth (sw11) before the July HW (Fig. 1h,i). This could have increased evaporative cooling; therefore favoring a lesser  $T_x$  amplification of the second heatwave in that specific area. In contrast, within the Pyrenees Mountain range itself, and mainly on its southern slope, the amplification of the July heatwave compared to the June heatwave was more than  $3^{\circ}\text{C}$  in some areas. Nevertheless, no significant variations in soil

175 moisture were observed between the two heatwaves (Fig. 1j), which indicates that such differences in the intensity of the events were not caused by diabatic mechanisms alone.



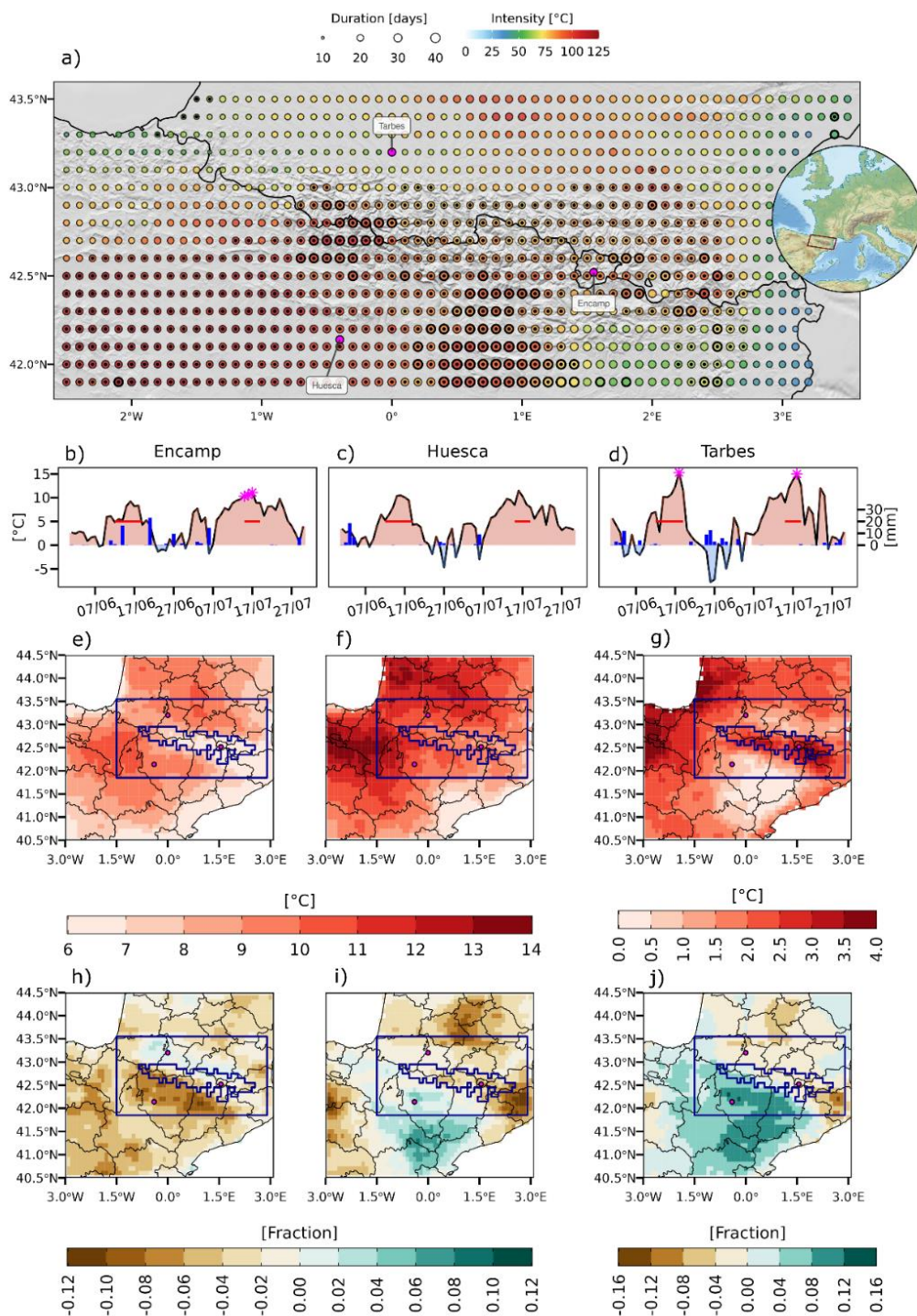
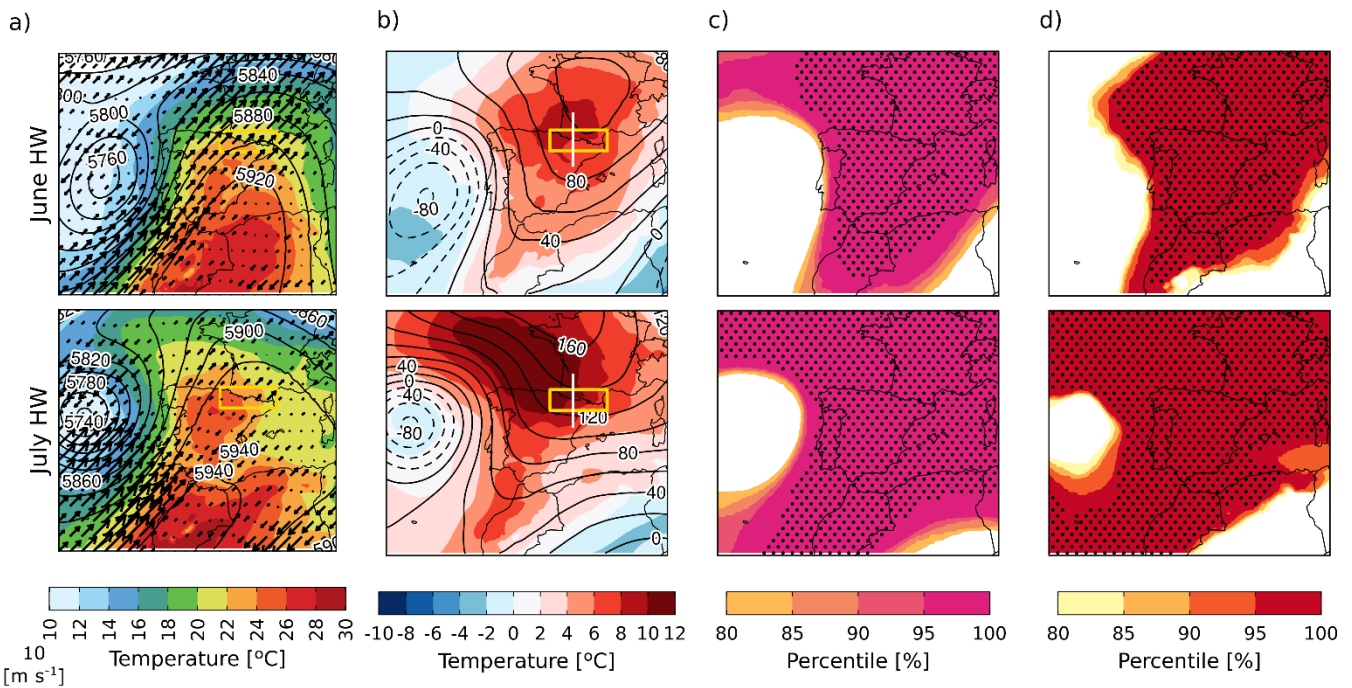


**Figure 1. Climatological description of the 2022 HW events in Pyrenees.** (a) Intensity (colours) and duration (sizes) of the summer 2022 (JJA). Dots inside the circle in (a) denote a record in intensity whereas thicker borders represent a record in duration for the period



185 1959–2021. (b,c,d) Timeseries of observed temperature anomalies (red and blue shaded) and precipitation (vertical bars) in Encamp, Huesca y Tarbes. Red horizontal lines represent the HW periods and magenta asterisks show absolute records. (e, f) Temperature anomalies during the (e) June HW, and (f) July HW and (g) the difference between July and June HWs. (h, i) soil water fraction anomaly in the first soil layer [0–7cm depth] (sw11,  $m^3 m^{-3}$ ) during the (h) June HW, and (i) July HW and (j) the difference between July and June HWs. Blue rectangle and region highlighted in e,f,g,h,i and j show the Pyrenean domain and the areas above 1000 m.a.s.l., respectively. Red points in the same panels indicate the location of Encamp, Huesca and Tarbes. Anomalies are calculated with respect to the period 1950–2021. Data source: ECAD, AEMET, FEDA and ERA5-Land.

190 Atmospheric dynamics could also partly explain the aforementioned temperature differences. (Fig. 2). The two main heatwaves of summer 2022 were driven by a deep subtropical ridge in the mid-troposphere (500 hPa) (Fig. 2a), resulting in exceptional geopotential height anomalies (Fig. 2b) over a large part of western Europe, consecutively breaking records (Fig. 2c). In both events, the 850 hPa temperature anomalies exceeded the 100th percentile across the Pyrenees area (Fig. 2d), implying a thermal anomaly between 6°C and up to 10°C at this pressure level (Fig. 2b). However, the July HW exhibited higher 500 hPa geopotential height anomalies than the June HW, with up to 40 meters of geopotential more. Furthermore, the 700 hPa wind field displayed a marked difference between the two episodes. The June heatwave was clearly dominated by strong south-western winds at mid and low levels, while in the second case the wind was much weaker and, therefore, the advection was lower.



200 **Figure 2. Mean Synoptic setting of the June and July HWs.** (a) Geopotential at 500 hPa (m, contours), temperature at 850 hPa (shaded) and wind at 700 hPa (arrows). (b) Geopotential at 500 hPa (m, contours) and temperature at 850 hPa (shaded) anomalies with respect to 1950–2021. (c,d) Percentile of (c) geopotential at 500 hPa and (d) temperature at 850 hPa, with respect to the climatological values calculated from a 6-day running mean of all summer days in the period 1950–2021. Stippling shows record breaking values. Top and



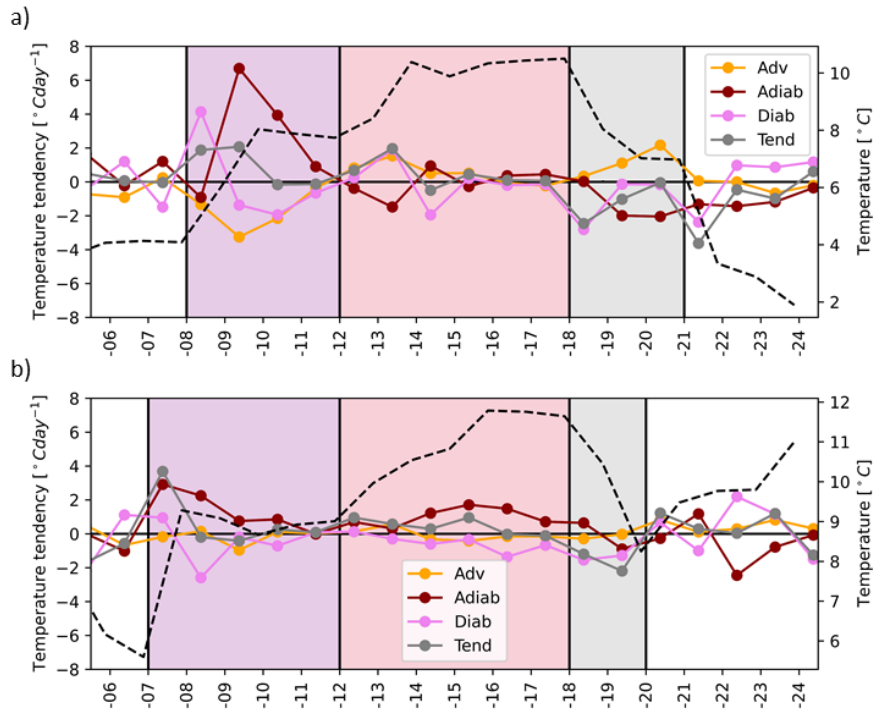


bottom rows show the June HW and July HW, respectively. The yellow box in (b) highlights the Pyrenean domain, whereas the vertical white line indicates the area used for the cross section in Fig. S2. Data source: ERA5.

### 205 3.2 Distinct physical processes led to different intensities for each heatwave in mountains.

As noted in the previous section, although both heatwaves were caused by subtropical ridges, they were dynamically different in terms of the physical processes leading to the Tx anomalies (Röthlisberger and Papritz, 2023). Specifically, the July event was more favorable for adiabatic processes due to the larger geopotential height anomalies combined with weak mid-low level winds, in contrast to the June HW, which had a more advective nature owing to the lower geopotential height values and the significantly stronger wind flow.

To better understand the different physical mechanisms that gave rise to the high temperatures in the Pyrenees region, we separately quantified the temperature trend due to adiabatic, diabatic and advective processes (Fig. 3). We conducted this analysis for both heatwaves at 700 hPa, to avoid the influence of the terrain in the analysis. For each heatwave we identified three phases. The first phase involved preconditioning, with a sudden temperature increase preceding the heatwave, providing a high baseline temperature. Adiabatic heating dominated this phase, indicating the importance of the ridge placement and associated subsidence for the subsequent heatwave development. During the build-up and maintenance phase, key processes differed between the heatwaves. The June heatwave was primarily driven by a warm advection during the first two days, associated with the southwesterly winds noted in the previous section. All components then remained almost neutral during the maintenance phase. In contrast, the July heatwave slowly developed over four days through adiabatic processes, with only two days of maintenance when the adiabatic warming decreased and was counteracted by diabatic cooling. Both heatwaves declined when the sum of components turned negative, resulting in a decrease in the absolute temperature tendency.



225 **Figure 3. Physical processes contributing to the summer 2022 heatwaves.** Time series in days from the beginning of the episode of the components of the heat tendency equation at 700 hPa during the (a) June HW and (b) July HW. Coloured lines indicate the temperature tendency for each component and dashed line indicates the temperature at 700 hPa. Shaded areas indicate the three phases of the heatwave: preconditioning (purple), build-up and maintenance (red) and decline (grey). Data source: ERA5.

230 The divergence in processes between the two heatwaves partially accounts for the varying amplification observed in the July HW compared with the June HW in the Pyrenees. During the June HW, higher horizontal wind speeds aloft generated mountain circulations characterized by updrafts on the windward side (south) and downdrafts on the leeward side of the Pyrenees (Fig. 4a). As a result, although advection caused a temperature increase across the entire region, the compression caused by the downdrafts on the leeside led to an increase of the temperature anomaly north to the Pyrenees (Fig. 4b). Conversely, the higher areas of the Pyrenees experienced less temperature anomalies during the June HW, due to windward updrafts to the mountain tops causing slight cooling by expansion; all of which led to a temperature gradient between both sides of the mountain range exceeding 3 degrees. In contrast, the July HW featured reduced atmospheric flow and more subsidence (Fig. 4c), resulting in a more homogeneous temperature distribution on both sides of the mountains and the absence of a cooling effect at the summits (Fig. 4d). This explains the amplification of the July HW over the Pyrenees with respect to the June HW observed in Fig. 1g, but cannot explain the low amplification that occurs in the Ebro valley south of  
240 the Pyrenees.

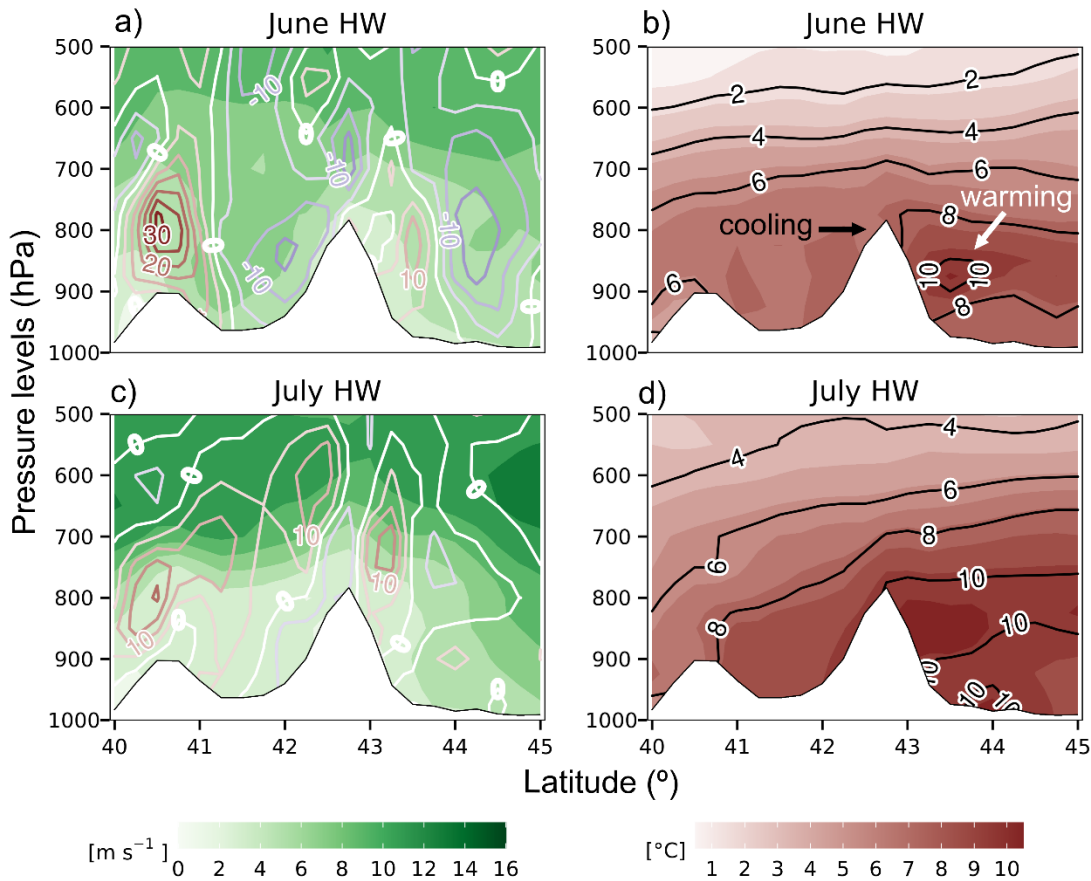


**Figure 4.** Cross-sections through the Pyrenees at longitude 0° during the June and July HW. On the left, Wind speed (shaded,  $\text{m s}^{-1}$ ) and vertical velocity (contours,  $\text{hPa day}^{-1}$ , negative values indicate updrafts) are shown for June (a) and July (b) heatwaves. (right) temperature anomalies (shaded,  $^{\circ}\text{C}$ ) and potential temperature anomalies (contours,  $^{\circ}\text{C}$ ). (top panels) June HW. (bottom panels) July HW.

245

### 3.3 Exploring the role of observed warming and soil moisture-temperature feedbacks by means of flow analogues

#### 3.3.1 Analysis of analogous situations

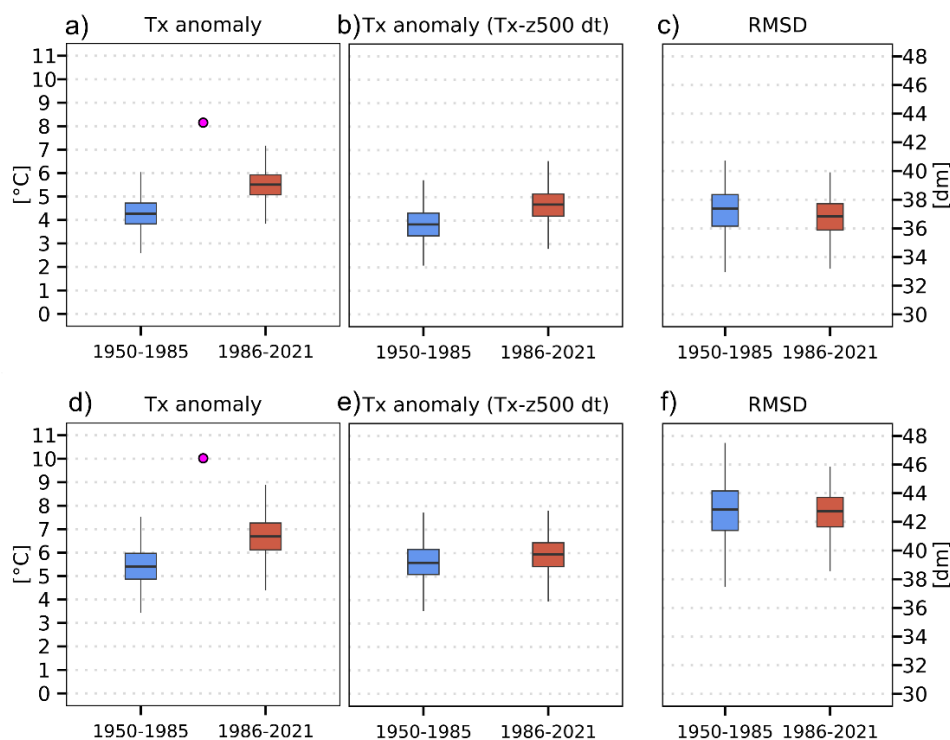
To investigate the role of climate change in the amplification of these heatwaves, we analyzed the 30 analogous days closest to the actual atmospheric configurations leading the cases studied. Specifically, we intercompare the Tx anomalies between the 30 circulation analogs in the more recent period (1986-2021) and 30 in the past period (1950-1985). These circulation analogs showed a temperature intensification for both the June and July HW events in the Pyrenees region (Fig. 5a,d); in both cases, the median Tx in the group of more recent analogs presented a Tx anomaly that clearly exceeded the anomalies reached in the group of past analogs by more than one degree.

An additional analysis was performed to check whether this temperature intensification could be to some extent caused by changes in the atmospheric circulation. In addition, to ensure that this amplification is caused by a pure thermodynamic

255



change between periods we removed the trend in both geopotential height and Tx (Sousa et al., 2019; Barriopedro et al., 2020), obtaining smaller differences between the two periods (Fig. 5b,e) compared with the previous experiment using raw data. Nevertheless, as can be seen, a certain bias remains between periods, especially in the June HW. We suggest that such differences notwithstanding the removal of the linear trend in both z500 and Tx, could be related to non-linear phenomena, such as the role of land-atmosphere interactions presented in the following section. The above shows that the temperature difference between the analogs of the two climate periods is mainly linked to a long-term trend in temperature. Assuming that this trend is largely due to global warming, this would indicate that the two heatwaves of 2022 were exacerbated by the observed anthropogenic warming, although some other non-linear processes could also have been involved.



265 **Figure 5. Flow-conditioned distributions of Tx daily mean anomaly reconstruction for each heatwave event (June: a-c; July: e-d)**  
**and for the Pyrenean domain [41.9°–43°N, 1.5°W–2.9°E].** (a,d) show the distributions obtained from raw data, (b,e) the distributions  
detrending z500 and Tx. The magenta dot in (a,d) denotes the mean value of observed Tx for each heatwave. (c,f) presents the spatial  
structure similarity between the reconstructed event and the original one based on z500. Boxes show the 25<sup>th</sup>–75<sup>th</sup> percentile ranges and  
whiskers span the 1<sup>st</sup>–99<sup>th</sup> percentiles. Blue and red boxes are representative of the past and current periods. Data source: ERA5-Land and  
270 ERA5 reanalysis.

Finally, it is important to point out that the spatial structure of our synoptic situations analogous to the June and July heatwaves remained similar in both periods (Fig. 5c,f) - which is consistent with other heatwave attribution studies in the western Mediterranean (Faranda et al., 2022) - and that their occurrence remained stationary, since we did not find a statistically significant trend in the number of analogs of both events in the period 1950-2021 (Fig. S2).



275

### 3.3.2 Contribution of soil-moisture temperature feedbacks

In the first section we had anticipated that between the two heatwaves precipitation had occurred south of the Pyrenees, thus increasing soil moisture, which could have reduced the temperature there in the July case via land-atmosphere feedbacks. This process, together with the orographic uplift already discussed, could explain the high spatial heterogeneity in the temperature anomalies of both heatwaves, as well as the thermal differences between the two events. Here we delve further into this issue using the analog method introduced in the previous section. At this point it is important to emphasize that, although we are considering analogues of the 2022 heatwaves in this section, we are not really analyzing the land-atmosphere feedback process for these specific cases, but we are investigating how this process works on average for many events analogous to the selected ones and how it is related to global warming.

First, we separated the analogs of both heatwaves into two periods (1950-1985 vs 1986-2021) and analyzed their Tx anomalies and the associated swll anomalies of the 15 days prior to the analog event (Fig. 6 and Fig. 7, See 2.2 for further details). The results show that the maximum level of Tx intensification in both heatwaves takes place on the southern slope of the Pyrenees (Spain) and in the Aquitaine basin (France) when comparing between the analogs of the current period with those of the past period (Fig. 6c and Fig. 7c). However, in the innermost area of the Pyrenees (1000 m.a.s.l. blue masked area), this enhancement reaches much lower values. We find that this pronounced pattern in the temperatures of analogs, which is corroborated by in-situ observations (Fig. S3 and Fig. S4), is highly correlated with the associated swll variability (Fig. 6f and Fig. 7f). For instance, the area of greatest temperature intensification south of the Pyrenees is also the region where moisture is most reduced in the present relative to the past. Likewise, the inner Pyrenees, where the temperature increase is lower, is one of the areas with less variation in soil moisture.

In addition, we studied the relationship between soil moisture change and temperature intensification in the most recent period using a land-atmosphere coupling metric (hereafter referred to as  $\pi$ ; see 2.2). Our calculations confirm the innermost Pyrenees as the area with the lowest coupling strengthening of the study region, especially during the July HW (Fig. 7g-h). But more importantly, the increase in Tx in the most recent period analogs has a high spatial coincidence with the increase of  $\pi$  (Fig. 6i and Fig. 7i), especially for the July case. This shows that the pattern of the temperature increase caused by the observed regional warming in the studied heatwaves is significantly modulated by soil-atmosphere feedbacks.



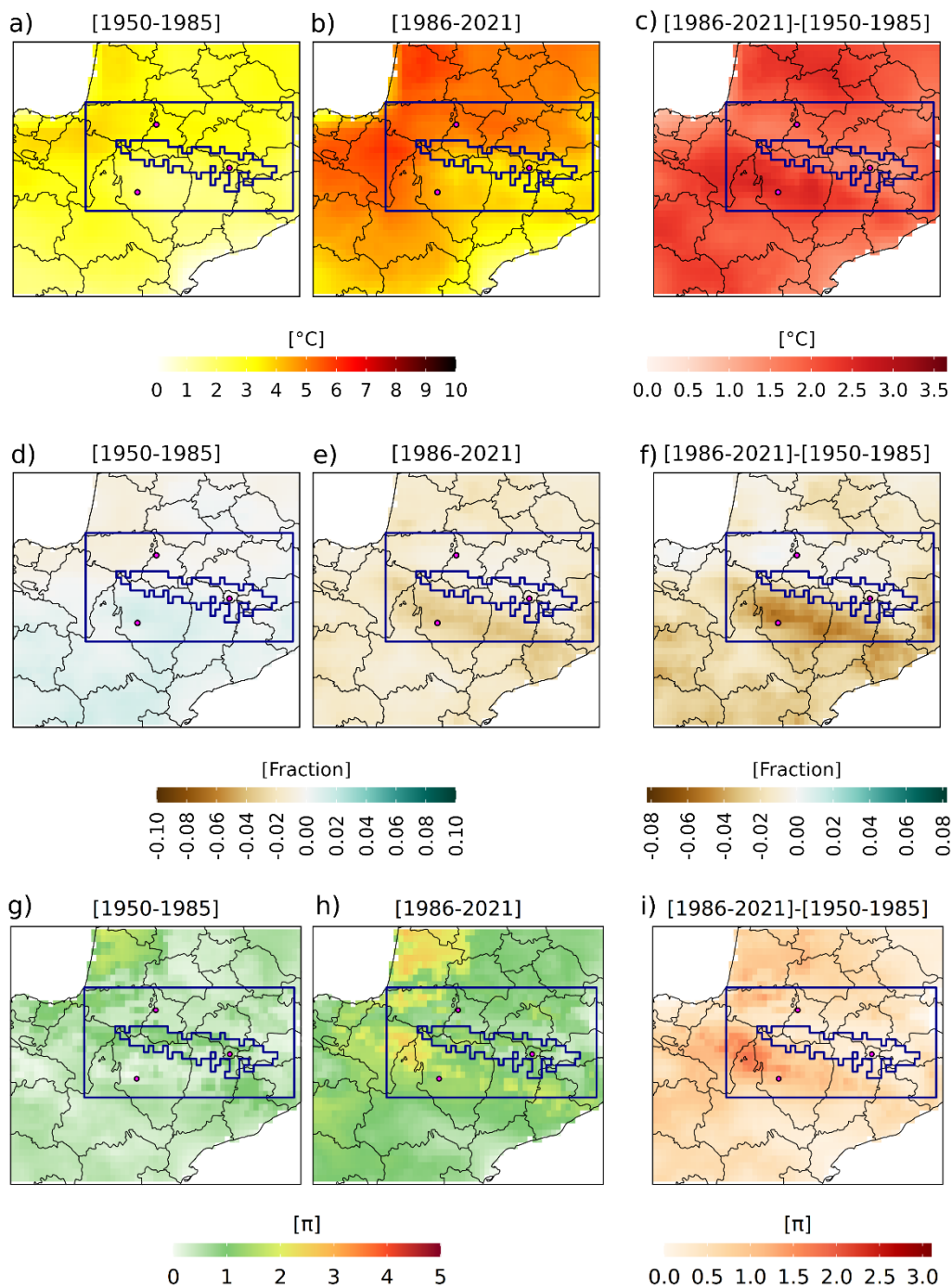


Figure 6. **June HW reconstruction by using past and present analogues.** Daily mean maximum 2m temperature ( $T_x$ ) anomalies (a), daily mean anomalies of soil moisture in the first soil layer [0-7cm] (sw1) (d) and soil moisture-temperature coupling metric  $\pi$  daily mean



305 (g) on the heatwave reconstruction in the past period [1950-1986]. (b),(e) and (h) as in (a), (d) and (g), respectively, but for the recent period [1986-2021]. (c), (f) and (i) show the difference between current and past periods for each respective variable. The anomalies in (a,b) and (d,e) were computed with respect to the period 1950-2021. Data source: ERA 5-Land.

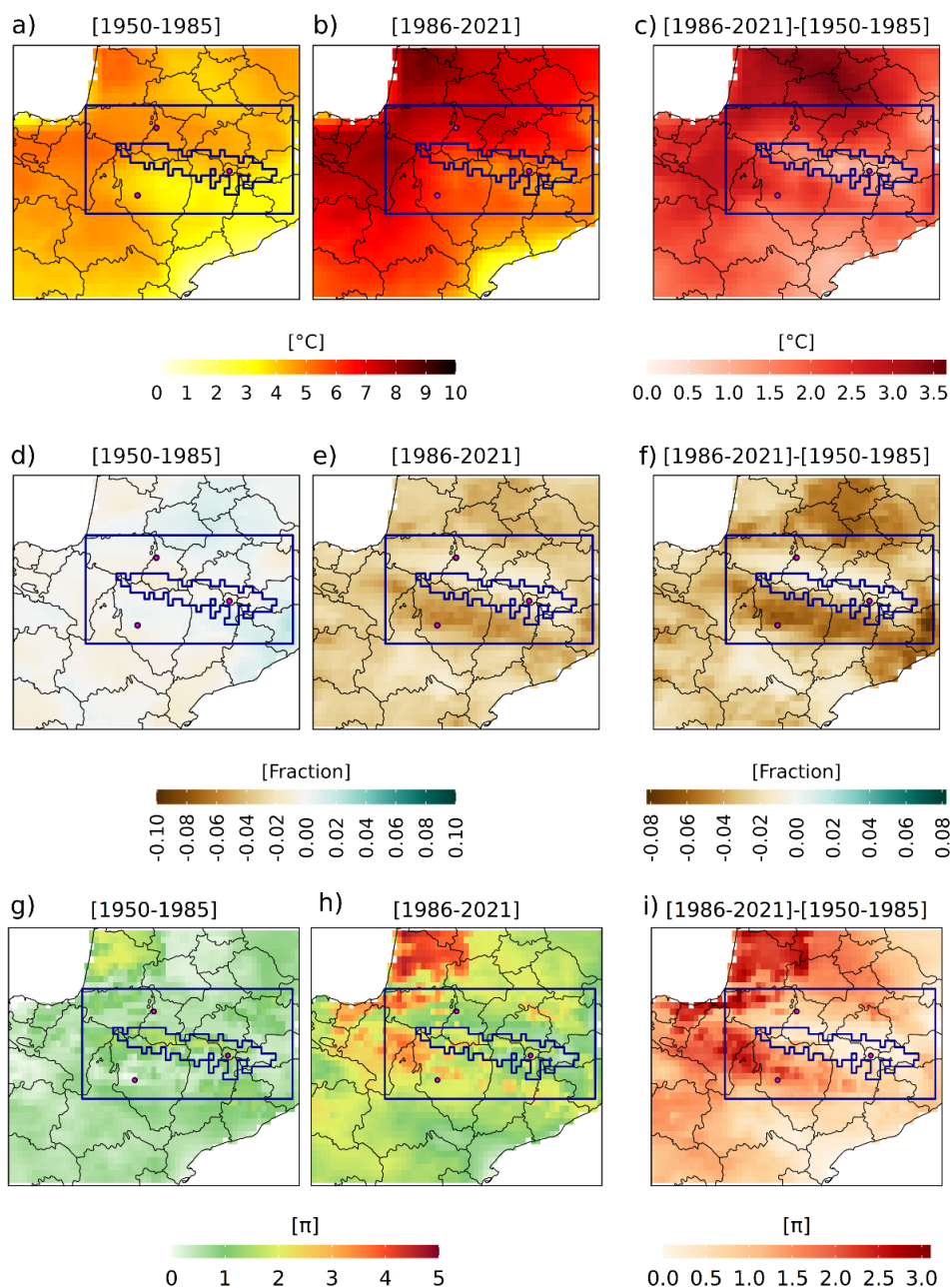
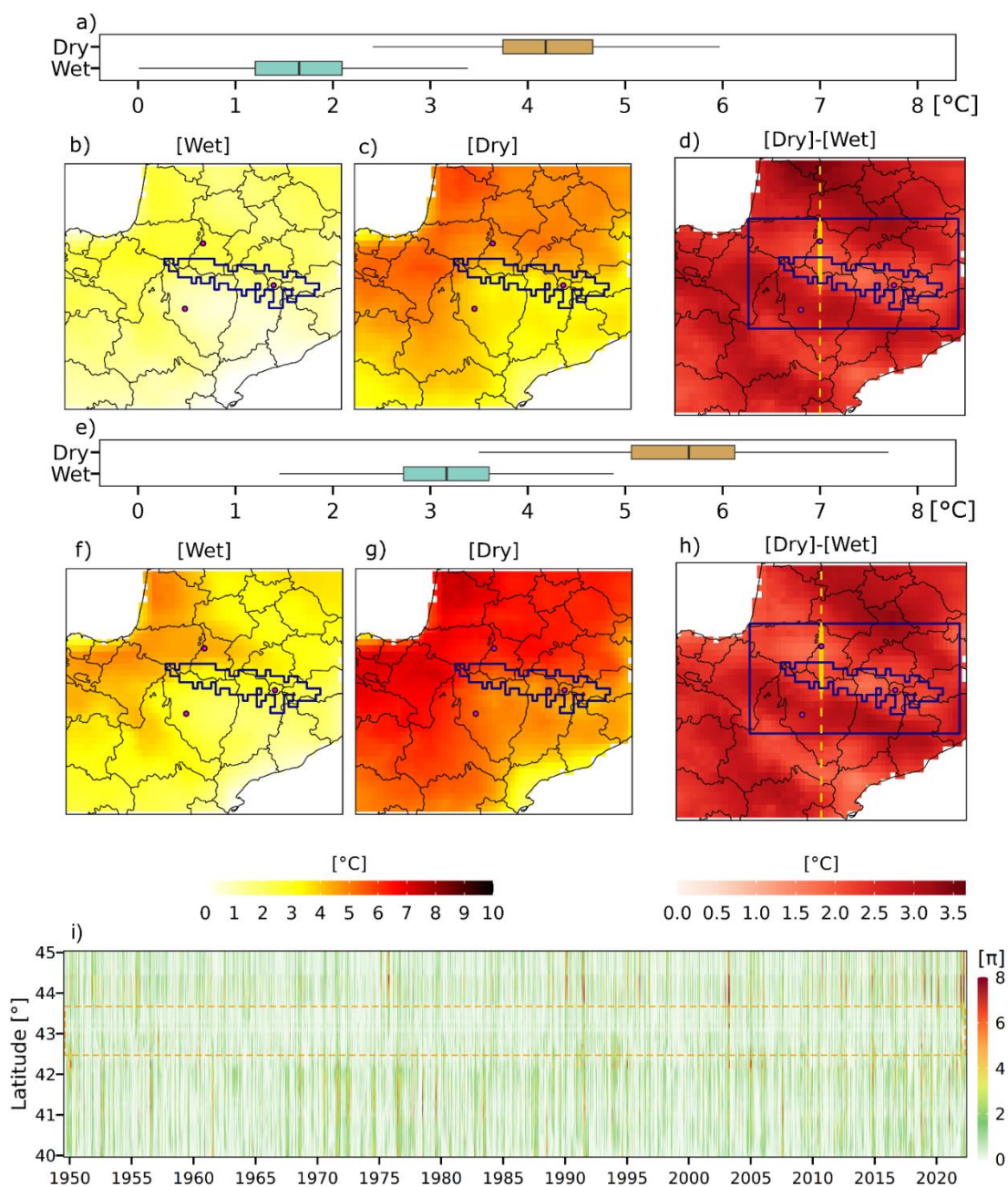


Figure 7. July HW reconstruction by using past and present analogues. Idem as Figure 6 but for the July HW



310 To corroborate the role of the soil moisture deficit in amplifying the intensity of the June HW and July HW, we split the  
analogue days into those preceded by dry conditions and those preceded by wet conditions over the Pyrenees domain,  
inferred from regional average anomalies of soil moisture over the previous 15 days (see 2.2). For this experiment we  
identified atmospheric circulation analogues for each day of each heatwave and reconstructed the Tx anomalies by removing  
the long-term trend from our data. The results indicate that 2022-like events preceded by dry conditions typically lead to  
315 warmer conditions (Fig. 8), higher than 2°C in terms of the difference between the median of both groups of analogues (Fig.  
8a,e). The field of Tx increase for both events (Fig. 8d,h) is again characterized by the highest values south of the Pyrenees  
and lower values in the interior of the mountain range. However, since we are working with detrended temperature and soil  
moisture data in this case, this cannot be attributed to a long-term variation in soil moisture caused by the observed  
anthropogenic warming. Thus, the wettest sector of the study area, corresponding to the highest altitudes and the northern  
320 slope of the mountain range (Fig. S5), also shows the lowest coupling (Fig. 8i), implying that varying the preconditions of  
soil moisture prior to a heatwave produces similarly high temperatures, in contrast to what is observed in the surrounding  
areas, which are affected by a much higher coupling (Fig. 8i). The aforementioned low thermal variation in the wettest part  
of the mountain range is also obtained when repeating the same experiment with a high-resolution gridded dataset specific to  
the Pyrenees for the period 1981-2015 (Fig. S6; See 2.2). The Ebro valley (most of which is outside the Pyrenean domain)  
325 also presents a low degree of coupling, as the temperature during the heatwave is weakly dependent on the prior soil  
moisture conditions, similar to what is found in the wettest area of the Pyrenees. However, in this case it is because of its  
extremely low soil moisture values during the warm season (Fig. S5), when the margin for soil dryness to cause temperature  
anomalies is limited, as dry soils are the norm there in summer.



330 **Figure 8. Wet and dry circulation analogues of the June and July heatwaves (HW).** (a) TX anomalies (with respect to 1950–2021) reconstructed for June (a-d) and July (e-h) HW (12–19 June 2022 and 15–19 July 2022, respectively) from daily flow analogues of Z500 over SW Europe preceded by (b,f) wet (above 66<sup>th</sup> percentile) and (c,g) dry (below 33<sup>rd</sup> percentile) soil moisture conditions at 0–7 cm in the Pyrenees domain (blue rectangular box in d,h) during the previous 15 days. d,h Difference between (c,g) and (b,f), respectively. (i)



335 Mean daily  $\pi$  coupling metric time series for a cross section at longitude  $0^\circ$  (yellow dashed line in d,h) for the summer seasons from 1950 to 2021. The inner dashed orange box refers to the region of lower coupling within the region marked by the thick yellow line in d,h.

#### 4 Discussion and conclusions

The summer of 2022 was extremely hot across the Pyrenees, both in terms of the duration of heatwaves and, more importantly in terms of their intensity. We used the HWMid indicator to detect the two most severe heatwaves that occurred in June and July, lasting 8 and 5 days, respectively, which broke some previous temperature records of the last 72 years, both at the surface (Tx) and at 850 hPa. Indeed, the HWMid values revealed the unprecedented nature of such heatwaves. In this study we i) presented the patterns of maximum temperature at 2m (Tx) and soil moisture in the first soil layer (sw11) during both events, ii) identified the synoptic patterns and the physical processes associated with the HWs; iii) quantified the role of the observed regional warming trend associated with the thermodynamic changes in June and July HW analogues; and finally, iv) showed how the precedent soil moisture conditions –through land-atmosphere interactions- can exacerbate the intensity of a June or July HW-like event.

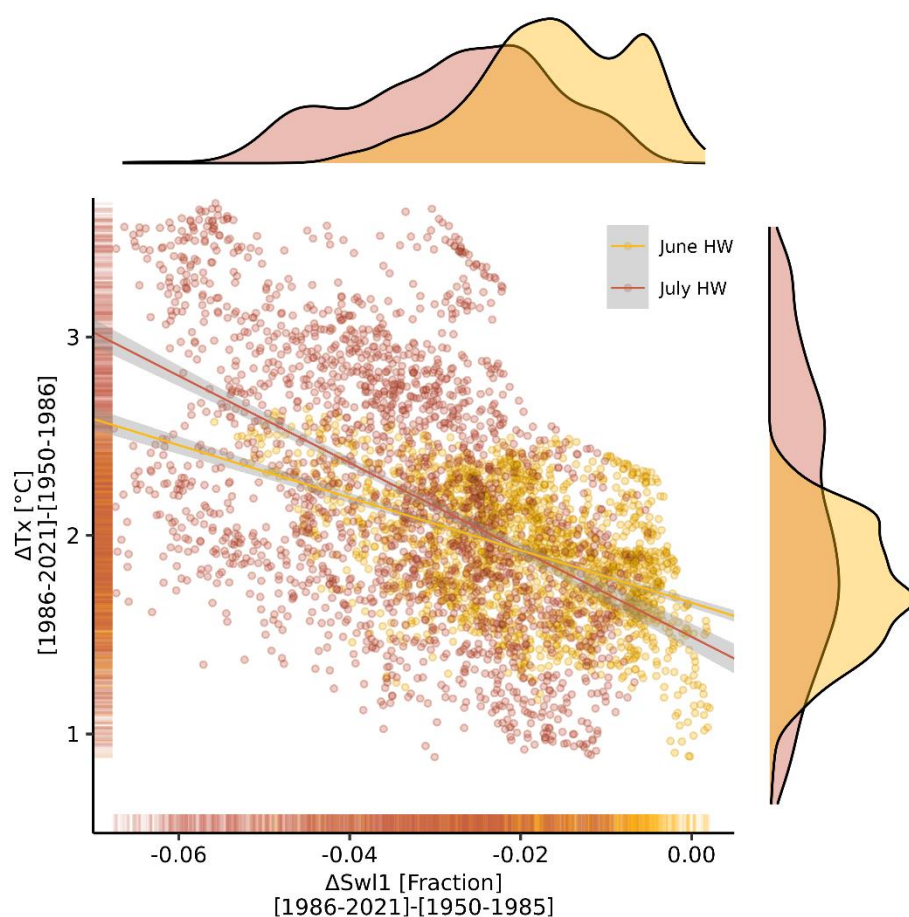
Different physical mechanisms were identified for the two HWs. Although adiabatic and diabatic warming are the most relevant physical processes determining HWs in Southern Europe (Zschenderlein et al., 2019; Röthlisberger and Papritz, 2023), the June HW was more advective in nature. This HW was driven by lower geopotential heights and stronger winds, which shaped the spatial distribution of the temperature anomalies. Higher horizontal wind speeds aloft generated mountain circulations with updrafts on the windward (south) side and downdrafts on the leeside (north) of the Pyrenees. This led to an increase in the temperature anomaly north of the Pyrenees, while reducing it at the mountain tops due to the cooling effect of the windward updrafts. Conversely, the July heatwave had larger geopotential height anomalies, decreased atmospheric flow and more subsidence, making it more conducive to adiabatic processes. Weaker mid- and low-level winds led to less mountain-induced circulations and thus, to a more uniform temperature distribution across the Pyrenees. These processes explained most of the differences observed between the two HWs and illustrate how mountain-induced circulations can regionally amplify or moderate HWs in their surroundings. The remaining differences can be attributed to land-atmosphere interactions, as discussed below.

Our findings also revealed a significant increase of the intensity of June or July heatwave-like events in the most recent period (1986-2021) compared with the past (1950-1985), with the thermodynamic component linked to human-induced global warming being the most relevant driver of this intensification. Thus, our results are in line with those presented for other recent heat events in Europe -also employing the flow analogue approach-, such as the Mediterranean heatwave of 2021 (Faranda et al., 2022), the Central European Heatwave of 2019 (Sousa et al., 2019), or the Iberian Peninsula heatwave of 2018 (Barriopedro et al., 2020), among others, although the latter studies focused on larger geographical areas and did not investigate the specific behaviour of heatwaves in mountain regions.





365 Our detailed attribution analysis over the Pyrenees showed that most areas in the domain are becoming drier prior to a  
heatwave occurrence in the most recent period. In fact, this moisture reduction was significantly correlated with a greater Tx  
increase in the most recent period ( $R_{\text{JuneHW}} = -0.30$ ;  $R_{\text{JulyHW}} = -0.71$ ; p-value  $< 0.01$ ; Fig. 9). Soil moisture anomalies  
reconstructed from circulation analogues, coincide with the negative observed trends of summer precipitation in the southern  
area of the Pyrenees (Perez-Zanon et al., 2017; Moreno et al., 2018), and annually for the same area (Lemus-Canovas et al.,  
370 2019). Similarly, other studies detected negative precipitation trends in the SW of France (Vidal et al., 2010; Philandras et  
al., 2011), generally without statistical significance. Such negative anomalies could also be aggravated by the more robust  
increase in temperature (Samaniego et al., 2018), which also leads to a further increase in potential evapotranspiration  
(Mastrotheodoros et al., 2020).



375 **Figure 9. Spatial relationship between changes in soil moisture and maximum temperatures for the June and July heatwave reconstructions.** Each dot in the scatter plot represents a grid point difference between 1986-2021 and 1950-1985 periods for both maximum daily temperature (Tx) and volumetric soil moisture fraction (swl1) 15-days prior to a heatwave (HW) event averaged reconstructions of the June (yellow) and July (red) HWs provided in Figure 6c and 6f, respectively. Marginal distributions are also shown



for each HW reconstruction and variable, with density color coding at the base of the axes, highlighting the concentration of data points.  
380 Linear regression lines reveal a positive correlation, suggesting that decreased soil moisture is associated with increased heatwave temperatures in both months, with a steeper gradient observed for July.

This observed drier trend in soil moisture was clearly greater in the southern part of the Pyrenean domain, which in turn was the area where a larger increase in Tx anomalies was observed in the analogue HW events belonging to the most recent period. Precisely, land-atmosphere coupling is widely recognised as a high temperature enhancer during heatwave episodes,  
385 both in this area of Europe (Felsche et al., 2023; Whan et al., 2015; Stefanon et al., 2012 and Della-Marta et al., 2007) and in other parts of the globe (Bartusek et al., 2022; Thompson et al., 2022; Rasmijn et al., 2018 and Hirschi et al., 2011). This study has also demonstrated that during heatwaves, land-atmosphere coupling strongly influences the spatial pattern of temperatures outside of the mountain areas. Notwithstanding the above, we reported several different temperature patterns across the Pyrenees that were less connected to soil moisture-temperature interactions. In fact, the inner and northern parts of  
390 the Pyrenees, which are the wettest sectors of the ridge, presented a low degree of coupling, thus being less sensitive to changes in soil moisture variations. These areas still present high soil moisture values regardless of whether they are drier than normal, which does not promote a substantial increase in sensible heat fluxes. In this regard, Stefanon et al. (2014) also detected a low soil moisture-temperature coupling both in the French Alps and in the Pyrenees during HW days of the period 1989-2008. They found lower temperature anomalies in the Alps compared with their surroundings in a dry soil scenario for  
395 the 2003 summer HW, suggesting that the combination of extreme heat and dry soils can lead to increased convection and cloud formation due to both anabatic winds (Jimenez et al., 2011) and a “dry advantage” regime (Ek and Holtslag, 2004; Gentine et al., 2012). Despite the reduced evaporation, the mixing of cold air from the boundary layer with the warmer air closer to the surface can increase relative humidity and facilitate the formation of clouds, especially shallow ones. Then, the lower amplification of Tx detected in the 2022 summer heatwave analogues in the most recent period, especially in the  
400 higher areas of the Pyrenees, due to the weaker land-atmosphere coupling, could be also favoured by the above-mentioned process of orographic cloud formation, being an additional factor limiting the temperature increase in this area in a warmer and drier Pyrenean scenario.

In conclusion, the observed regional warming tends to amplify events like the June and July HWs throughout the Pyrenees, but mountain-induced circulations in advective HWs can modify the temperature anomaly distribution in mountain areas.  
405 Advective type HWs, on the other hand, might present a more homogeneous warming across the region. In this case, regional soil desiccation may amplify the magnitude of this type of events by creating certain sub-regional hotspots (e.g., the southern Pyrenees). At the same time, wet areas show less land-atmosphere interaction and are therefore less affected by the cascading events connecting drought with high temperatures. Although the study of the role of land-atmosphere interactions in exacerbating heatwave intensity is not new, the current study allowed to derive a more detailed relationship between soil  
410 desiccation and the observed increase in heatwave temperature in an area of complex topography where the coupling effects vary greatly. Further research is needed to extend our understanding of the underlying physical mechanisms at the mesoscale



to other temperate mountain regions, towards a comprehensive view of the changing dynamics of weather extremes in a warming world.

### Data availability

415 All data used in this study is accessible online via the following links: ERA5 dataset:

<https://www.ecmwf.int/en/forecasts/datasets/reanalysis-datasets/era5>.

ERA5-Land dataset: <https://www.ecmwf.int/en/forecasts/datasets/reanalysis-datasets/era-20c>.

CLIMPY dataset: <https://zenodo.org/records/3611127>

Huesca and Tarbes in situ weather stations: ecad.eu. Encamp time series: meteo.ad

### 420 Code availability

All codes used in this study are available upon a reasonable request after publication.

### Author contribution

M.L.-C. designed the experiments, conducted the data analysis, and wrote the first draft of the manuscript. S.G.-H. led the analysis of the physical processes contributing to the heatwave events and prepared Figure 3. All authors contributed to writing the article, provided ideas, helped interpret the results, and participated in revising the manuscript.

425

### Competing interests

The authors declare that they have no known competing financial interests or personal relationships that could have appeared to influence the work reported in this paper.

### Acknowledgements

430 M.L.-C. is supported by a postdoctoral contract from the program named “Programa de axudas de apoio á etapa inicial de formación posdoutoral (2022)” funded by Xunta de Galicia (Government of Galicia, Spain). Reference number: ED481B-2022-055. M.L.-C. has been also supported by a postdoctoral contract from Andorra Research & Innovation (2021). S.G.-H. was supported by the research group ANTALP (Antarctic, Arctic, Alpine Environments; 2021 SGR 00269) funded by the Agència de Gestió d'Ajuts Universitaris i de Recerca of the Government of Catalonia. D.I.-C. is supported by the European Space Agency (ESA) grant no. 4000136272/21/I-EF (CCN. N.1), 4D-MED Hydrology. M.S.-R. is funded by the Spanish Ministry of Science and Innovation through the RIESPIRO research project (PID2021-128510OB-I00).

435



## References

- Barriopedro, D., Sousa, P.M., Trigo, R.M., García-Herrera, R., Ramos, A.M., 2020. The Exceptional Iberian Heatwave of Summer 2018. *Bulletin of the American Meteorological Society* 101, S29–S34. <https://doi.org/10.1175/BAMS-D-19-0159.1>
- 440 Bartusek, S., Kornhuber, K., Ting, M., 2022. 2021 North American heatwave amplified by climate change-driven nonlinear interactions. *Nat. Clim. Chang.* 12, 1143–1150. <https://doi.org/10.1038/s41558-022-01520-4>
- Camarero, J.J., 2017. The Multiple Factors Explaining Decline in Mountain Forests: Historical Logging and Warming-Related Drought Stress is Causing Silver-Fir Dieback in the Aragón Pyrenees, in: Catalan, J., Ninot, J.M., Aniz, M.M. (Eds.), *High Mountain Conservation in a Changing World*. Springer International Publishing, Cham, pp. 131–154.
- 445 [https://doi.org/10.1007/978-3-319-55982-7\\_6](https://doi.org/10.1007/978-3-319-55982-7_6)
- Cremona, A., Huss, M., Landmann, J.M., Borner, J., Farinotti, D., 2023. European heat waves 2022: contribution to extreme glacier melt in Switzerland inferred from automated ablation readings. *The Cryosphere* 17, 1895–1912. <https://doi.org/10.5194/tc-17-1895-2023>
- Cuadrat, J.M., Serrano-Notivol, R., Tejedor, E., Saz, M.Á., Prohom, M., Cunillera, J., Llabrés, A., Trapero, L., Pons, M., 450 López-Moreno, J.I., Copons, R., Gascoin, S., Luna, Y., Rodríguez, E., Ramos, P., Amblar, P., Soubeyroux, J.-M., 2020. CLIMPY: Climate of the Pyrenees. <https://doi.org/10.5281/zenodo.3611127>
- Della-Marta, P.M., Haylock, M.R., Luterbacher, J., Wanner, H., 2007. Doubled length of western European summer heat waves since 1880. *J. Geophys. Res.* 112, 2007JD008510. <https://doi.org/10.1029/2007JD008510>
- Ek, M.B., Holtslag, A. a. M., 2004. Influence of Soil Moisture on Boundary Layer Cloud Development. *Journal of* 455 *Hydrometeorology* 5, 86–99. [https://doi.org/10.1175/1525-7541\(2004\)005<0086:IOSMOB>2.0.CO;2](https://doi.org/10.1175/1525-7541(2004)005<0086:IOSMOB>2.0.CO;2)
- Faranda, D., Bourdin, S., Ginesta, M., Krouma, M., Noyelle, R., Pons, F., Yiou, P., Messori, G., 2022. A climate-change attribution retrospective of some impactful weather extremes of 2021. *Weather and Climate Dynamics* 3, 1311–1340. <https://doi.org/10.5194/wcd-3-1311-2022>
- Felsche, E., Böhnisch, A., Ludwig, R., 2023. Inter-seasonal connection of typical European heatwave patterns to soil 460 moisture. *npj Clim Atmos Sci* 6, 1–11. <https://doi.org/10.1038/s41612-023-00330-5>
- Fischer, E.M., Seneviratne, S.I., Lüthi, D., Schär, C., 2007. Contribution of land-atmosphere coupling to recent European summer heat waves. *Geophysical Research Letters* 34, 2006GL029068. <https://doi.org/10.1029/2006GL029068>
- García-Herrera, R., Díaz, J., Trigo, R.M., Hernández, E., 2005. Extreme summer temperatures in Iberia: health impacts and associated synoptic conditions. *Annales Geophysicae* 23, 239–251. <https://doi.org/10.5194/angeo-23-239-2005>
- 465 Gazol, A., Sangüesa-Barreda, G., Camarero, J.J., 2020. Forecasting Forest Vulnerability to Drought in Pyrenean Silver Fir Forests Showing Dieback. *Front. For. Glob. Change* 3, 36. <https://doi.org/10.3389/ffgc.2020.00036>
- Gentine, P., D’Odorico, P., Lintner, B.R., Sivandran, G., Salvucci, G., 2012. Interdependence of climate, soil, and vegetation as constrained by the Budyko curve. *Geophysical Research Letters* 39, 2012GL053492. <https://doi.org/10.1029/2012GL053492>



- 470 González-Herrero, S., Barriopedro, D., Trigo, R.M., López-Bustins, J.A., Oliva, M., 2022. Climate warming amplified the 2020 record-breaking heatwave in the Antarctic Peninsula. *Commun Earth Environ* 3, 1–9. <https://doi.org/10.1038/s43247-022-00450-5>
- Hersbach, H., Bell, B., Berrisford, P., Hirahara, S., Horányi, A., Muñoz-Sabater, J., Nicolas, J., Peubey, C., Radu, R., Schepers, D., Simmons, A., Soci, C., Abdalla, S., Abellan, X., Balsamo, G., Bechtold, P., Biavati, G., Bidlot, J., Bonavita,  
475 M., De Chiara, G., Dahlgren, P., Dee, D., Diamantakis, M., Dragani, R., Flemming, J., Forbes, R., Fuentes, M., Geer, A., Haimberger, L., Healy, S., Hogan, R.J., Hólm, E., Janisková, M., Keeley, S., Laloyaux, P., Lopez, P., Lupu, C., Radnoti, G., De Rosnay, P., Rozum, I., Vamborg, F., Villaume, S., Thépaut, J., 2020. The ERA5 global reanalysis. *Quart J Royal Meteorol Soc* 146, 1999–2049. <https://doi.org/10.1002/qj.3803>
- Hirschi, M., Seneviratne, S.I., Alexandrov, V., Boberg, F., Boroneant, C., Christensen, O.B., Formayer, H., Orłowsky, B.,  
480 Stepanek, P., 2011. Observational evidence for soil-moisture impact on hot extremes in southeastern Europe. *Nature Geosci* 4, 17–21. <https://doi.org/10.1038/ngeo1032>
- Jézéquel, A., Yiou, P., Radanovics, S., 2018. Role of circulation in European heatwaves using flow analogues. *Clim Dyn* 50, 1145–1159. <https://doi.org/10.1007/s00382-017-3667-0>
- Jiménez, P.A., Arellano, J.V.-G. de, González-Rouco, J.F., Navarro, J., Montávez, J.P., García-Bustamante, E., Dudhia, J.,  
485 2011. The Effect of Heat Waves and Drought on Surface Wind Circulations in the Northeast of the Iberian Peninsula during the Summer of 2003. *Journal of Climate* 24, 5416–5422. <https://doi.org/10.1175/2011JCLI4061.1>
- Lemus-Canovas, M., Lopez-Bustins, J.A., 2021. Assessing internal changes in the future structure of dry-hot compound events: the case of the Pyrenees. *Natural Hazards and Earth System Sciences* 21, 1721–1738. <https://doi.org/10.5194/nhess-21-1721-2021>
- 490 Lemus-Canovas, M., Lopez-Bustins, J.A., Trapero, L., Martin-Vide, J., 2019. Combining circulation weather types and daily precipitation modelling to derive climatic precipitation regions in the Pyrenees. *Atmospheric Research* 220, 181–193. <https://doi.org/10.1016/j.atmosres.2019.01.018>
- López-Moreno, J.I., Gascoin, S., Herrero, J., Sproles, E.A., Pons, M., Alonso-González, E., Hanich, L., Boudhar, A., Musselman, K.N., Molotch, N.P., Sickman, J., Pomeroy, J., 2017. Different sensitivities of snowpacks to warming in  
495 Mediterranean climate mountain areas. *Environ. Res. Lett.* 12, 074006. <https://doi.org/10.1088/1748-9326/aa70cb>
- López-Moreno, J.I., Revuelto, J., Rico, I., Chueca-Cía, J., Julián, A., Serreta, A., Serrano, E., Vicente-Serrano, S.M., Azorin-Molina, C., Alonso-González, E., García-Ruiz, J.M., 2016. Thinning of the Monte Perdido Glacier in the Spanish Pyrenees since 1981. *The Cryosphere* 10, 681–694. <https://doi.org/10.5194/tc-10-681-2016>
- Mastrotheodoros, T., Pappas, C., Molnar, P., Burlando, P., Manoli, G., Parajka, J., Rigon, R., Szeles, B., Bottazzi, M.,  
500 Hadjidoukas, P., Fatichi, S., 2020. More green and less blue water in the Alps during warmer summers. *Nat. Clim. Chang.* 10, 155–161. <https://doi.org/10.1038/s41558-019-0676-5>





- Miralles, D.G., Teuling, A.J., van Heerwaarden, C.C., Vilà-Guerau de Arellano, J., 2014. Mega-heatwave temperatures due to combined soil desiccation and atmospheric heat accumulation. *Nature Geosci* 7, 345–349. <https://doi.org/10.1038/ngeo2141>
- 505 Miralles, D.G., van den Berg, M.J., Teuling, A.J., de Jeu, R. a. M., 2012. Soil moisture-temperature coupling: A multiscale observational analysis. *Geophysical Research Letters* 39. <https://doi.org/10.1029/2012GL053703>
- Moreno, A., Valero-Garcés, B.L., Verfaillie, D., Galop, D., Rodríguez Camino, E., Tejedor, E., Barreiro Lostres, F., Soubeyroux, J.-M., Cunillera, J., Cuadrat, J.M., García Ruiz, J.M., López Moreno, J.I., Trapero, L., Pons, M., Prohom Duran, M., Saz Sánchez, M.Á., González Sampéris, P., Ramos Calzado, P., Amblar, M.P., Copons, R., Serrano Notivoli, R.,
- 510 Gascoïn, S., Luna Rico, Y., 2018. Clima y variabilidad climática en los Pirineos. OPCC-CTP.
- Muñoz-Sabater, J., Dutra, E., Agustí-Panareda, A., Albergel, C., Arduini, G., Balsamo, G., Boussetta, S., Choulga, M., Harrigan, S., Hersbach, H., Martens, B., Miralles, D.G., Piles, M., Rodríguez-Fernández, N.J., Zsoter, E., Buontempo, C., Thépaut, J.-N., 2021. ERA5-Land: a state-of-the-art global reanalysis dataset for land applications. *Earth System Science Data* 13, 4349–4383. <https://doi.org/10.5194/essd-13-4349-2021>
- 515 Pérez-Zanón, N., Sigró, J., Ashcroft, L., 2017. Temperature and precipitation regional climate series over the central Pyrenees during 1910–2013. *Intl Journal of Climatology* 37, 1922–1937. <https://doi.org/10.1002/joc.4823>
- Philandras, C.M., Nastos, P.T., Kapsomenakis, J., Douvis, K.C., Tselioudis, G., Zerefos, C.S., 2011. Long term precipitation trends and variability within the Mediterranean region. *Natural Hazards and Earth System Sciences* 11, 3235–3250. <https://doi.org/10.5194/nhess-11-3235-2011>
- 520 Priestley, C.H.B., Taylor, R.J., 1972. On the Assessment of Surface Heat Flux and Evaporation Using Large-Scale Parameters. *Monthly Weather Review* 100, 81–92. [https://doi.org/10.1175/1520-0493\(1972\)100<0081:OTAOSH>2.3.CO;2](https://doi.org/10.1175/1520-0493(1972)100<0081:OTAOSH>2.3.CO;2)
- Rasmijn, L.M., van der Schrier, G., Bintanja, R., Barkmeijer, J., Sterl, A., Hazeleger, W., 2018. Future equivalent of 2010 Russian heatwave intensified by weakening soil moisture constraints. *Nature Clim Change* 8, 381–385. <https://doi.org/10.1038/s41558-018-0114-0>
- 525 Rodrigues, M., Cunill Camprubí, À., Balaguer-Romano, R., Coco Megía, C.J., Castañares, F., Ruffault, J., Fernandes, P.M., Resco de Dios, V., 2023. Drivers and implications of the extreme 2022 wildfire season in Southwest Europe. *Science of The Total Environment* 859, 160320. <https://doi.org/10.1016/j.scitotenv.2022.160320>
- Röthlisberger, M., Papritz, L., 2023. Quantifying the physical processes leading to atmospheric hot extremes at a global scale. *Nat. Geosci.* 16, 210–216. <https://doi.org/10.1038/s41561-023-01126-1>
- 530 Russo, S., Dosio, A., Graversen, R.G., Sillmann, J., Carrao, H., Dunbar, M.B., Singleton, A., Montagna, P., Barbola, P., Vogt, J.V., 2014. Magnitude of extreme heat waves in present climate and their projection in a warming world. *JGR Atmospheres* 119. <https://doi.org/10.1002/2014JD022098>
- Samaniego, L., Thober, S., Kumar, R., Wanders, N., Rakovec, O., Pan, M., Zink, M., Sheffield, J., Wood, E.F., Marx, A., 2018. Anthropogenic warming exacerbates European soil moisture droughts. *Nature Clim Change* 8, 421–426. <https://doi.org/10.1038/s41558-018-0138-5>
- 535



- Schumacher, D.L., Keune, J., van Heerwaarden, C.C., Vilà-Guerau de Arellano, J., Teuling, A.J., Miralles, D.G., 2019. Amplification of mega-heatwaves through heat torrents fuelled by upwind drought. *Nat. Geosci.* 12, 712–717. <https://doi.org/10.1038/s41561-019-0431-6>
- 540 Seneviratne, S.I., Corti, T., Davin, E.L., Hirschi, M., Jaeger, E.B., Lehner, I., Orlowsky, B., Teuling, A.J., 2010. Investigating soil moisture–climate interactions in a changing climate: A review. *Earth-Science Reviews* 99, 125–161. <https://doi.org/10.1016/j.earscirev.2010.02.004>
- Serrano-Notivoli, R., Beguería, S., de Luis, M., 2019. STEAD: a high-resolution daily gridded temperature dataset for Spain. *Earth System Science Data* 11, 1171–1188. <https://doi.org/10.5194/essd-11-1171-2019>
- 545 Serrano-Notivoli, R., Beguería, S., Saz, M.Á., Longares, L.A., de Luis, M., 2017. SPREAD: a high-resolution daily gridded precipitation dataset for Spain – an extreme events frequency and intensity overview. *Earth System Science Data* 9, 721–738. <https://doi.org/10.5194/essd-9-721-2017>
- Serrano-Notivoli, R., Tejedor, E., Sarricolea, P., Meseguer-Ruiz, O., de Luis, M., Saz, M.Á., Longares, L.A., Olcina, J., 2023. Unprecedented warmth: A look at Spain’s exceptional summer of 2022. *Atmospheric Research* 293, 106931. <https://doi.org/10.1016/j.atmosres.2023.106931>
- 550 Sousa, P.M., Barriopedro, D., García-Herrera, R., Ordóñez, C., Soares, P.M.M., Trigo, R.M., 2020. Distinct influences of large-scale circulation and regional feedbacks in two exceptional 2019 European heatwaves. *Commun Earth Environ* 1, 1–13. <https://doi.org/10.1038/s43247-020-00048-9>
- Sousa, P.M., Barriopedro, D., Ramos, A.M., García-Herrera, R., Espírito-Santo, F., Trigo, R.M., 2019. Saharan air intrusions as a relevant mechanism for Iberian heatwaves: The record breaking events of August 2018 and June 2019. *Weather and Climate Extremes* 26, 100224. <https://doi.org/10.1016/j.wace.2019.100224>
- 555 Sousa, P.M., Trigo, R.M., Barriopedro, D., Soares, P.M.M., Santos, J.A., 2018. European temperature responses to blocking and ridge regional patterns. *Clim Dyn* 50, 457–477. <https://doi.org/10.1007/s00382-017-3620-2>
- Stefanon, M., D’Andrea, F., Drobinski, P., 2012. Heatwave classification over Europe and the Mediterranean region. *Environ. Res. Lett.* 7, 014023. <https://doi.org/10.1088/1748-9326/7/1/014023>
- 560 Stéfanon, M., Drobinski, P., D’Andrea, F., Lebeaupin-Brossier, C., Bastin, S., 2014. Soil moisture-temperature feedbacks at meso-scale during summer heat waves over Western Europe. *Clim Dyn* 42, 1309–1324. <https://doi.org/10.1007/s00382-013-1794-9>
- Thompson, V., Kennedy-Asser, A.T., Vosper, E., Lo, Y.T.E., Huntingford, C., Andrews, O., Collins, M., Hegerl, G.C., Mitchell, D., 2022. The 2021 western North America heat wave among the most extreme events ever recorded globally. *Sci. Adv.* 8, eabm6860. <https://doi.org/10.1126/sciadv.abm6860>
- 565 Vidal, J., Martin, E., Franchistéguy, L., Baillon, M., Soubeyroux, J., 2010. A 50-year high-resolution atmospheric reanalysis over France with the Safran system. *Intl Journal of Climatology* 30, 1627–1644. <https://doi.org/10.1002/joc.2003>



- Vidaller, I., Revuelto, J., Izagirre, E., Rojas-Heredia, F., Alonso-González, E., Gascoin, S., René, P., Berthier, E., Rico, I., Moreno, A., Serrano, E., Serreta, A., López-Moreno, J.I., 2021. Toward an Ice-Free Mountain Range: Demise of Pyrenean  
570 Glaciers During 2011–2020. *Geophysical Research Letters* 48, e2021GL094339. <https://doi.org/10.1029/2021GL094339>
- Whan, K., Zscheischler, J., Orth, R., Shongwe, M., Rahimi, M., Asare, E.O., Seneviratne, S.I., 2015. Impact of soil moisture on extreme maximum temperatures in Europe. *Weather and Climate Extremes, The World Climate Research Program Grand Challenge on Extremes – WCRP-ICTP Summer School on Attribution and Prediction of Extreme Events* 9, 57–67. <https://doi.org/10.1016/j.wace.2015.05.001>
- 575 White, R.H., Anderson, S., Booth, J.F., Braich, G., Draeger, C., Fei, C., Harley, C.D.G., Henderson, S.B., Jakob, M., Lau, C.-A., Mareshet Admasu, L., Narinesingh, V., Rodell, C., Roocroft, E., Weinberger, K.R., West, G., 2023. The unprecedented Pacific Northwest heatwave of June 2021. *Nat Commun* 14, 727. <https://doi.org/10.1038/s41467-023-36289-3>
- Witze, A., 2022. Extreme heatwaves: surprising lessons from the record warmth. *Nature* 608, 464–465. <https://doi.org/10.1038/d41586-022-02114-y>
- 580 Xu, P., Wang, L., Huang, P., Chen, W., 2021. Disentangling dynamical and thermodynamical contributions to the record-breaking heatwave over Central Europe in June 2019. *Atmospheric Research* 252, 105446. <https://doi.org/10.1016/j.atmosres.2020.105446>
- Yule, E.L., Hegerl, G., Schurer, A., Hawkins, E., n.d. Using early extremes to place the 2022 UK heat waves into historical  
585 context. *Atmospheric Science Letters* n/a, e1159. <https://doi.org/10.1002/asl.1159>
- Zschenderlein, P., Fink, A.H., Pfahl, S., Wernli, H., 2019. Processes determining heat waves across different European climates. *Quart J Royal Meteorol Soc* 145, 2973–2989. <https://doi.org/10.1002/qj.3599>